CORE
Metadata, citation and similar papers at core.ac.uk
Provided by CaltechCONF

Comparison of Cavitation Phenomena in Transparent Scaled-up Single-Hole Diesel Nozzles

L. C. Ganippa, G. Bark, S. Andersson and J. Chomiak
Chalmers University of Technology, Sweden

Abstract

The structure and evolution of cavitation in a transparent scaled-up diesel nozzle having a hole inclined at 90, 85, 80 and 0 degree to the nozzle axis has been investigated using high-speed motion pictures, flash photography and stroboscopic visualization. Observations revealed that at the inception stage, cavitation bubbles were not seen at the same locations in all the four nozzles. Cavitation bubbles grew intensively and developed into cloud-like structures. Shedding of the cloud cavitation was observed. When the flow was increased further the cloud-like cavitation bubbles developed into a dense large-scale cavitation cloud extending downstream of the hole. Under this condition the cavitation started mainly as a glassy sheet at the entrance of the hole. Until this stage the spray appeared to be symmetric. When the flow was increased beyond this stage, a sheet of cavitation covered a significant part of the hole on one side, extending to the hole exit. This non-symmetric distribution of cavitation within the hole resulted in a jet, which atomized on the side where more cavitation was distributed and non-atomizing on the side with less cavitation. The distribution of cavitation in the hole was different for different nozzles.

1 Introduction

The fuel injection system of a diesel engine plays a crucial role in reducing exhaust emissions by determining the spray formation ignition and combustion. The spray formation and in particular atomization process is highly complex owing to the underlying physical processes in the nozzle internal flow and the environment into which the spray is injected. It is believed that cavitation could be a possible contributor to the spray break-up at the nozzle exit.

At low upstream pressures, Bergwerk (1959) observed the nozzle hole to run full except for a cavity at the upstream corner. Increasing the pressure causes the cavities to extend throughout the hole, increasing the ruffles of the spray and causing a sudden transition in the appearance of the jet from ruffled to smooth and glass-like, together with a change in the discharge coefficient under certain limit conditions. The cavity formation was found to be a function of the cavitation number ($CN = (P_1-P_2)/P_2$, where P_1 and P_2 are the absolute upstream and downstream pressures and the vapour pressure is neglected). Reitz *et al.* (1982) proposed that, among the other factors such as turbulence, surface instability etc., which contribute to the aerodynamic break-up, cavitation phenomena are a dominant factor, which complement the aerodynamic effects. Hiroyasu *et al.* (1991) observed that the jet break-up length was shortened due to cavitation fixed at the nozzle entrance and the break-up length increased when the vapour cavity at the hole walls was too strong to be disrupted in the nozzle, which resulted in a non-atomizing smooth jet.

Studies have been carried out by Kato *et al.* (1997) to measure the pressure distribution in the nozzle sac and discharge hole. Their observation revealed that cavitation at the hole inlet is very sensitive to the nozzle sac geometry and the injection hole configuration. Badock *et al.* (1998) investigated the cavitation phenomena in the spray hole of a real-size diesel injection nozzle. They observed cavitation films inside the spray hole using the light sheet technique and were also able to see the core of the flow, which was covered by cavitation films. Cavitation films between the flow and the nozzle wall, as well as single cavitation bubbles could be observed at different times of the injection process. No foam or small bubbles were noticed in the spray hole.

The internal flow structure in a scaled-up plain orifice nozzle was studied by Soteriou *et al.* (1999) using a laser light sheet. They observed incipient cavitation at three distinct locations *viz.*, (i) in the separated boundary layer, *i.e.* just down stream of the entrance, (ii) in the main stream flow and (iii) within the attached boundary layer, *i.e.* all along the walls of the orifice downstream of the separated boundary layer and extending out of the orifice. Plug cavitation was identified in the development process. As the plug cavitation reached the hole exit a sudden increase in spray angle was observed. This plug cavitation was not observed at lower Reynolds numbers. At the inception stage

shedding of cavitation was observed, and this shedding was speculated to give an increased spray angle at the inception stage. Kim *et al.* (1997) visualized the flow in the sac chamber and the discharge hole of a scaled-up two-hole acrylic nozzle. At small needle lifts they observed a spiral air cavity at the exit of the discharge hole, which developed in the upstream direction of the flow into the sac. These typical spiral air cavities from both the holes were linked with each other at the tip of the needle valve. The spiral air cavity in the sac developed into a thread-like shape, which in time changed into a cavitation film flowing out of the sac chamber into the discharge hole. This phenomenon occurred repeatedly and caused a fluctuation in the spray angle. However, this was not observed at higher needle lifts characteristic of normal, fully opened operation.

A transparent, six-hole, scaled-up model nozzle was used to visualize the flow effects by matching both the Reynolds number and cavitation number to that of the real-size diesel nozzle by, Arcoumanis *et al.* (1999). Their investigation revealed two different types of cavitation, (i) cavitation originating at the entrance to the injector hole and (ii) cavitation strings developed in the sac volume. The cavitation strings link adjacent holes and interact with the pre-existing cavitation to result in chaotic discharge variations. The strings were not consistently uniform in each hole, which resulted in hole-to-hole variations. An extension of this work to a real-size multi-hole was reported in Arcoumanis *et al.* (2000), where geometry-induced cavitation and string cavitation were also observed in a real-size injector. A similar form of string cavitation was also observed by Walther *et al.* (2000) in a real-size 3-hole nozzle. The experimental investigation of Chaves *et al.* (1996) revealed that the spray angle of a nozzle is a weak function of injection pressure beyond a limit discharge rate.

In the present work a simple nozzle of diesel-like geometry with varying hole inclination was used to investigate the influence of the internal nozzle flow on the spray dispersion. A comparison is made of the cavitation pattern prevailing in each of the four nozzles.

2 Experimental set-up

The schematic of the experimental set-up used to investigate the internal nozzle flow and spray structure is shown in Figure 1. Throughout the experiments, tests were done with water as the working fluid. The set-up consists of a water supply system which supplies water to the first tank, from which it was further transported to the main reservoir through a flow control valve. In order to maintain a low air content in the working fluid, a vacuum pump was connected to the main water tank. The working fluid was driven by a gear pump. The pumped fluid passes through a filter and reaches the settling chamber upstream of the nozzle. In order to avoid any preferential direction of flow in the settling chamber, a flat stagnation plate was used at the entrance. The level of turbulence in the settling chamber is reduced by forcing the fluid through a honeycomb.

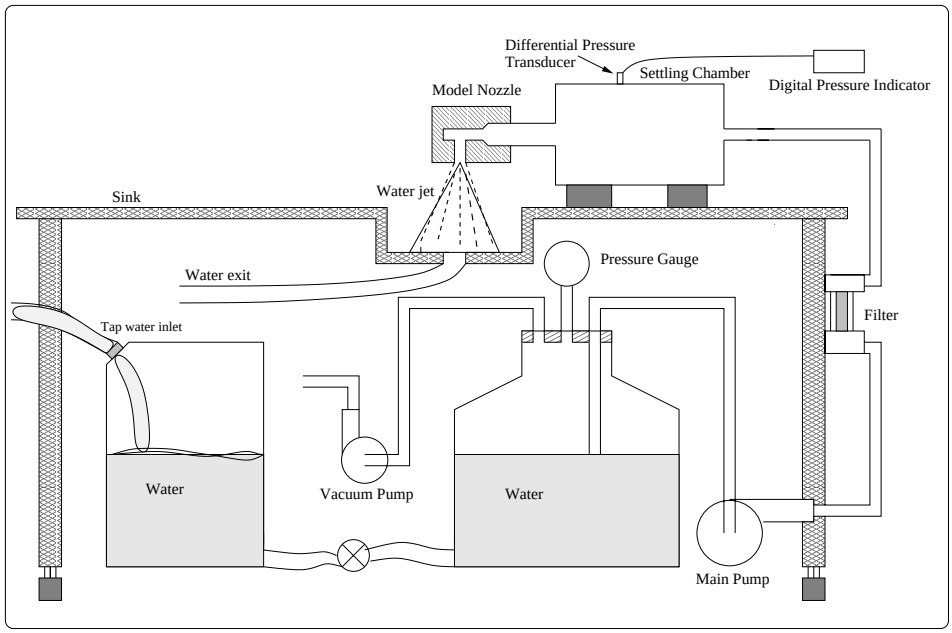

Figure 1. Schematic of the test rig.

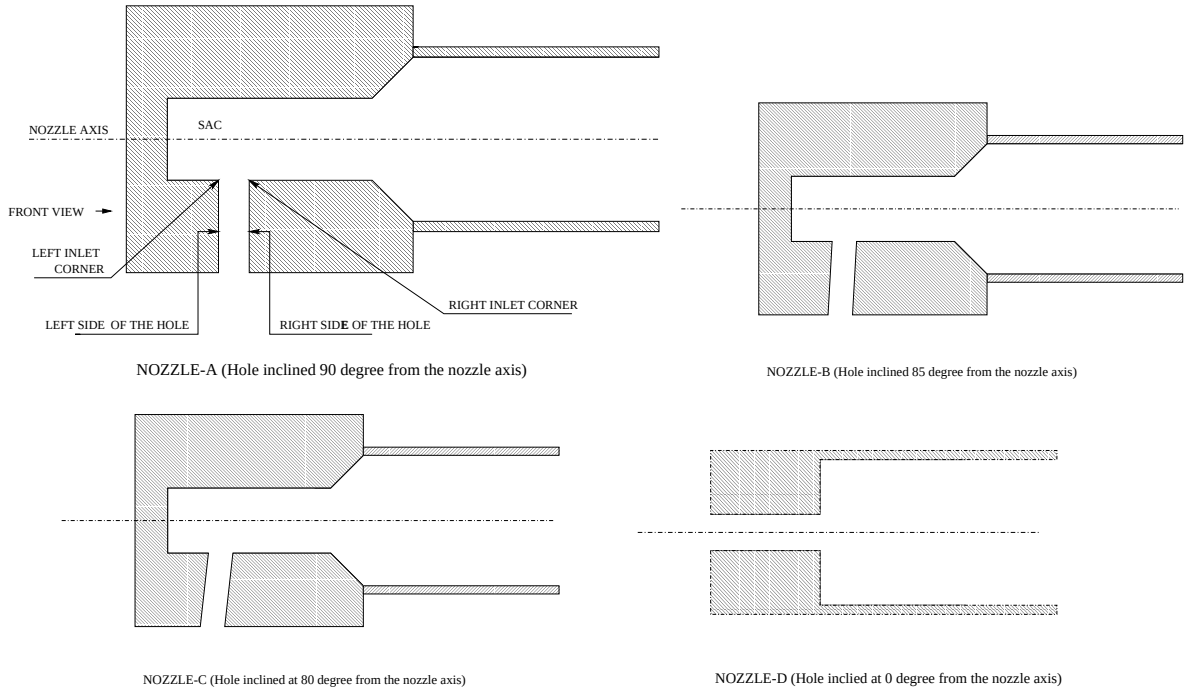

Figure 2. Model nozzles of various hole inclinations

The pressure drop across the nozzle was measured using a differential pressure transducer mounted on the settling chamber. Experiments were done with Reynolds numbers (based on the orifice diameter of 4.7mm) ranging from $40x10^3$ to $100x10^3$. The complex cavitation phenomena occurring in the nozzle, Figure 2, were captured using a HYCAM high-speed 16-mm motion picture camera. In the current work the cavitating flow in the nozzle was pictured at 8000 frames per second. To acquire the required brightness, the nozzle was illuminated from above using a 1.2 kW HMI light. To have a three-dimensional view of the cavitation in the nozzle, pictures were taken from the front and side of the nozzle. Apart from high-speed visualization, the cavitation and the spray pictures were taken using a 35-mm still camera with a flash duration of 28 μs.

3 Cavitation flow visualization

Cavitation Inception - The observations indicate that in the inception stage the cavitation bubbles were seen at different position in all the four nozzles. In nozzle-A the inception bubbles are generated at the sharp right inlet corner and these bubbles are occasionally seen at the inlet corner. Most of the nuclei then grow and coagulate in the turbulent vortices generated in the shear layer and also outside the separation zone downstream of the hole inlet as shown in Figure 4 (a). Thus the inception bubbles are more clearly seen in the vortices of the shear boundary layer. Occasionally the nuclei grow directly at the sharp inlet corner. Close to the inception condition the observations made on the nozzle-A show that the cavitation bubbles travel with the flow and are not in contact with the wall of the nozzle due to the vortex structure present in the boundary shear layer as well as the large separation bubble, *i.e.* the re-circulation zone which is quite large for nozzle-A. In nozzle-B the inception bubbles are seen both on the right and left inlet corner as shown in Figure 7 (a). The separation bubble on the right inlet side is large compared to the left inlet side. Thus the inception bubbles seen on the right inlet corner are mostly separated from the wall and found on the vortices present in the shear boundary layer. The inception bubbles seen on the left inlet side are closer to the wall compared to the inception bubbles seen on the right inlet side. In nozzle-C the inception bubbles are seen only on the left inlet corner, Figure 10 (a), which is quite different from the above two nozzles. The cavitation bubbles are close to the wall and are not separated from the wall like nozzle-A. The nozzle-D is symmetric about its axis. Thus the inception occurs all through the circumference of the hole inlet which is quite different from all the other three nozzles where the inception bubbles are not seen all around the hole inlet. The inception photograph of nozzle-D is shown in Figure 12 (a). The photographs taken from the front side of the nozzle-A, nozzle-B and nozzle-C at the inception condition demonstrate that, the bubbles are distributed over a span of the nozzle diameter, at some downstream distance, from the inlet corner as seen in Figure 3 (a), Figure 6 (a) and Figure 9 (a) respectively.

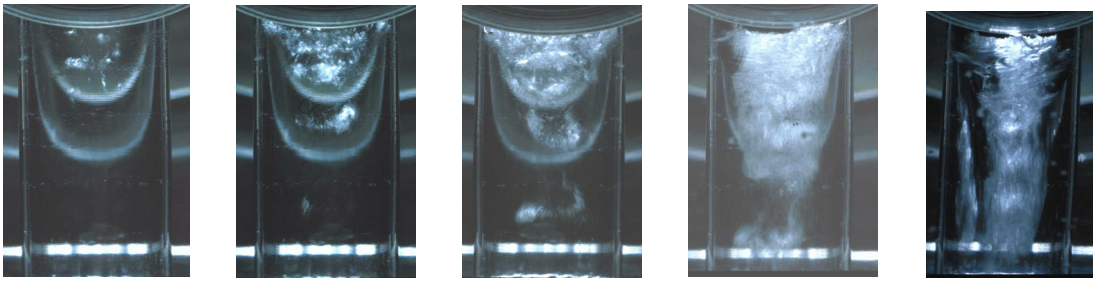

(a) (b) (c) (d) (e)

Figure 3. Front view of nozzle-A

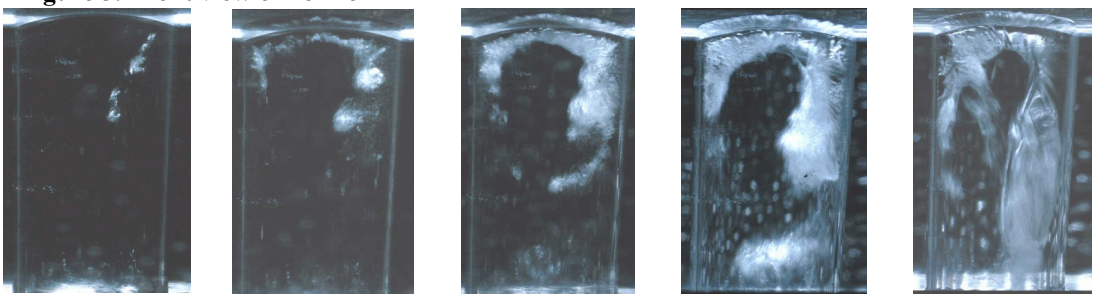

(a) (b) (c) (d) (e)

Figure 4. Side view of nozzle-A

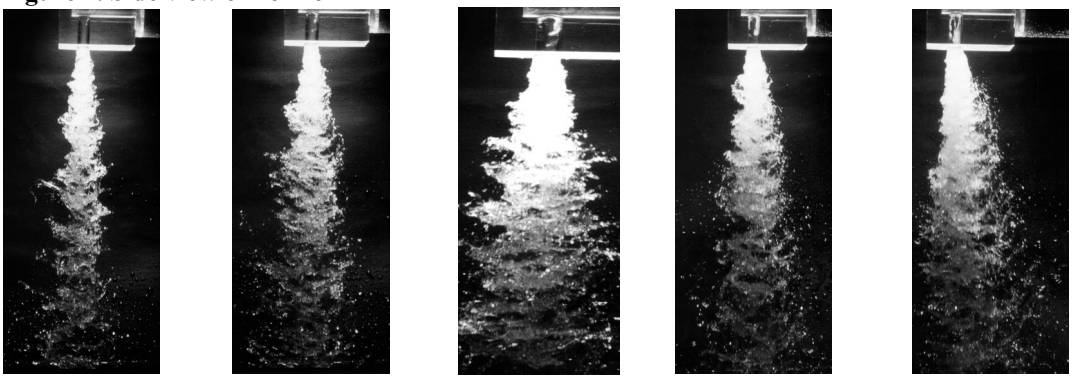

(a) (b) (c) (d) (e)

Figure 5. Spray dispersion from nozzle-A

(a) incipient cavitation; (b) developing cloud; (c) developed coherent cavitation; (d) developed coherent cavitation on both sides; (e) glossy sheet cavitation stage

Even though the inception locations in all the four nozzles are different, there exist some similarities in the cavitation pattern in the nozzles. During the inception stage, the cavitation is of travelling bubble type. Inception nuclei are generated at the sharp inlet corners; occasionally the nuclei grow fast enough to be seen directly at the sharp inlet corners. These cavities disappear before reaching one-fourth of the nozzle hole length. The Reynolds number based on the sac diameter reveals that the flow at the hole entrance is not laminar under these conditions.

Developing Cloud Cavitation - When the flow is increased, the cavitation bubbles are seen both on the right and left inlet of nozzle-A (Figure 4 (b)), nozzle-B (Figure 7 (b)) and nozzle-C, (Figure 10 (b)) respectively. The isolated bubbles of travelling type seen in the inception stage are no longer visible. The bubbles seen inside and outside the shear layer of nozzle-A, nozzle-B and nozzle-C grow intensively and tend to form a cloud-like structure in shear induced turbulent vortices, a behaviour similar to those vortices was visualized and reported by Taneda (2000) and O'Hern (1991). In this condition, small bubbles are seen in the re-circulation zone, which could have been the bubbles that are transported from the bubble cloud present in the vortices of the shear layer. More cavitation is seen on the right inlet corner compared to the left inlet corner of nozzle-A. The cloud cavitation tends to develop coherent perturbation structures. After breakoff, the shed cavitation cloud is transported towards the centre of the hole.

The front views, Figures 3 (b), Figure 6 (b) and Figure 9 (b), show as before, that cavitation appears to be distributed densely over the span of the nozzle, approaching the shape of a tongue with the tongue base at the upstream right and left inlet corner and the tongue tip suspended in the main flow. The cloud cavitation developing in the vortices of the turbulent shear layer lies within the tongue extending from the inlet corner in nozzle-A and nozzle-B. In the front view of nozzle-A, nozzle-B and nozzle-C the optical effect in a form of a continuous bowline should not be misinterpreted as part of the cavitation tongue. The cavitation clouds that are shed seldom survived until the hole exit. No cavitation bubbles are observed at the hole inlet circumference other than the one observed on the right and left inlet corners.

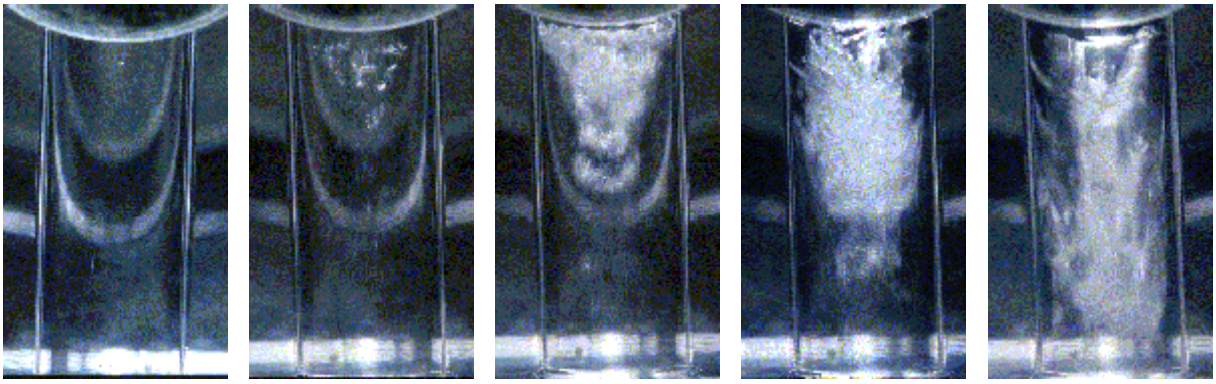

(a) (b) (c) (d) (e)

Figure 6. Front view of nozzle-B

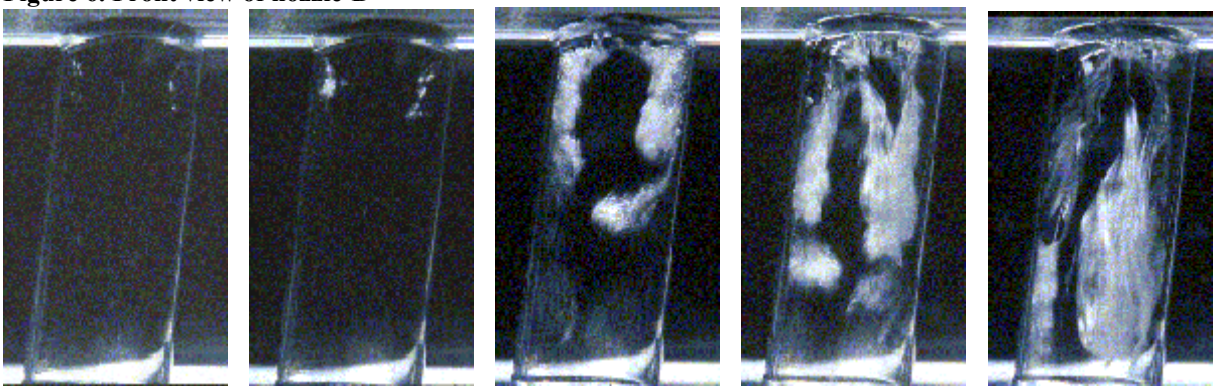

(a) (b) (c) (d) (e)

Figure 7. Side view of nozzle-B

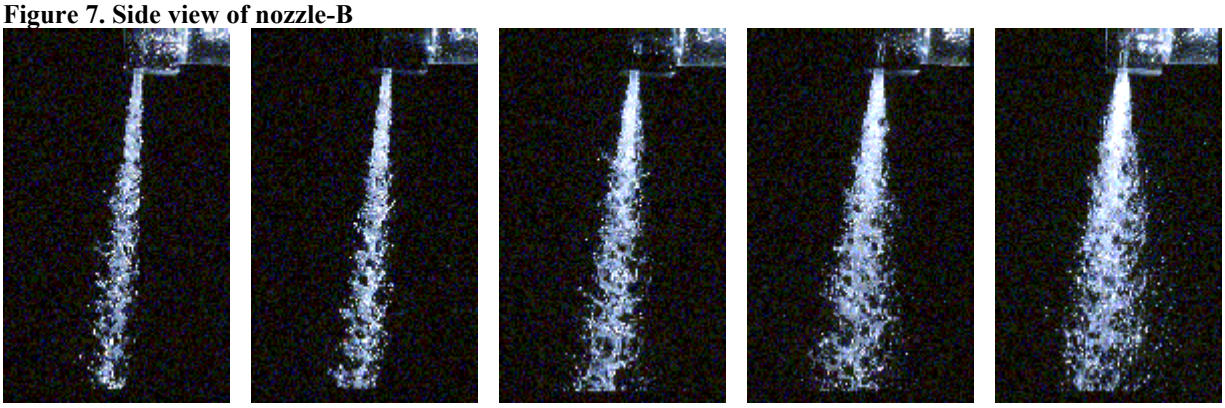

(a) (b) (c) (d) (e)

Figure 8. Spray dispersion from nozzle-B

(a) incipient cavitation; (b) developing cloud; (c) developed coherent cavitation; (d) developed coherent cavitation on both sides; (e) glossy sheet cavitation stage

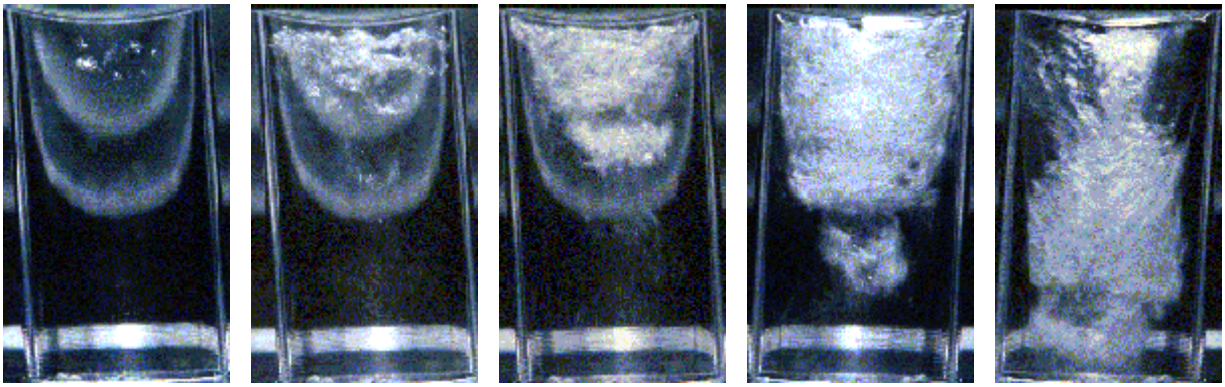

(a) (b) (c) (d) (e)

Figure 9. Front view of nozzle-C

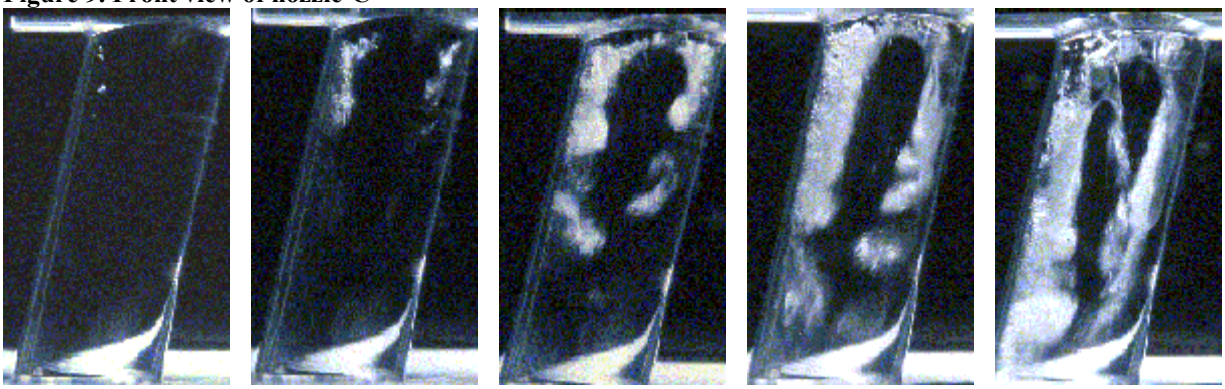

(a) (b) (c) (d) (e)

Figure 10. Side view of nozzle-C

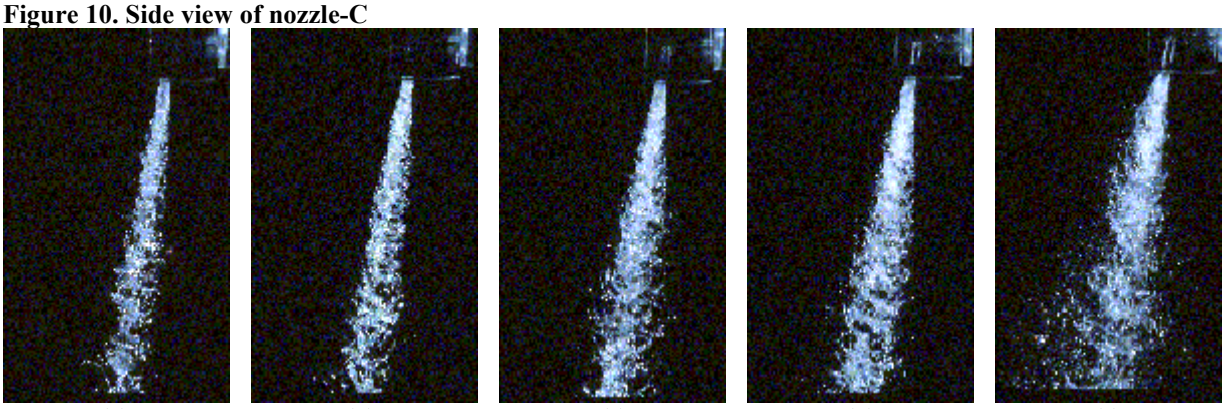

(a) (b) (c) (d) (e)

Figure 11. Spray dispersion from nozzle-C
(a) incipient cavitation; (b) developing cloud; (c) developed coherent cavitation;
(d) developed coherent cavitation on both sides; (e) glossy sheet cavitation stage

Developed Coherent Structure - In this stage, the cavitation appears as a dense cloud like large-scale coherent structure on the right side of the hole and a similar coherent cavitation cloud structure on the left side but of smaller size in nozzle-A, Figure 4 (c). In nozzle-B, Figure 7 (c), the dense cavitation clouds are seen both on the right and left sides. The cavitation clouds are distributed more on the right side compared to the left side. In Nozzle-C, Figure 10 (c), the cloud cavitation is distributed more on the left side of the hole compared to the right side, which is quite opposite to the cavitation distribution in the above two nozzles.

Despite the differences in the distribution of the cavitation cloud in the nozzles, some similarities are seen *i.e.* in this stage, the instabilities developed in the vortices of the shear layer causes the large-scale structures to break off. This results in a periodic shedding of the large-scale structures of cavitation cloud from both the sides of the nozzle hole. The shed large-scale cavitation appears to be in the form of vortex rings of the horseshoe type, which is clearly seen,

in the front view of nozzle-A (Figure 3 (c)) and nozzle-B (Figure 6 (c) respectively. Vortex ring structures are not clearly seen in nozzle-C because the cavitation cloud is distributed more on the left side of the hole, Figure 9 (c). In this stage the shedding of the cavitation cloud is seen in all the nozzles even before the half-length of the nozzle hole. Cavitation is seen in the circumference of the hole inlet, which was not seen in the previous stages.

As the flow was increased beyond this level, the large-scale structures extended towards the downstream edge of the hole as seen in Figure 4 (d), Figure 7 (d) and Figure 10 (d) respectively. Besides the developed large-scale coherent structure found on either side, there are also cloudy strips of cavitation present within the flowing fluid. Shedding is observed in this stage, but vortex ring structures are not seen due to the breakoff of the cloud occurring downstream close to the hole exit. When viewed from the side, cloudy strips within the hole attaching the existing coherent cloud at the hole inlet circumference were seen but when viewed from the front no definite structures could be seen except for a cloud like structure breaking off from a big cloud as shown in Figure 3 (d), Figure 6 (d) and Figure 9 (d) respectively.

The cavitation developed in nozzle-D is quite different from other nozzles. Due to the axisymmtric geometry the cavitation originates at the hole inlet circumference. It grows intensively and transforms into a dense cloud. Shedding is observed in this stage. As the flow is increased it is observed that the cloud travels downstream of the hole oscillating about the exit position and it is connected to the hole inlet through a sheet having a complex turbulent structure as seen in Figure 12 (d).

Glossy Sheet Structure –Traces of a glossy sheet could be seen at the hole entrance even at the developed stages, *i.e.* in Figure 4(d), Figure 7(d) and Figure 10(d), while the rest of it was cloud cavitation in all the four nozzles. It was also seen that in particular for nozzle-A, B and C the sheet not only originated at the left and right inlet corners of the hole but all around the hole circumference. This effect caused the glossy sheet to look twisted under higher flow conditions, Figure 4 (e), Figure 7 (e), and Figure 10 (e) when viewed from the side. When viewed from front of the hole just a glossy sheet like structure with cloudy structures was observed as shown in Figure 3 (e), Figure 6 (e) and Figure 9 (e) respectively.

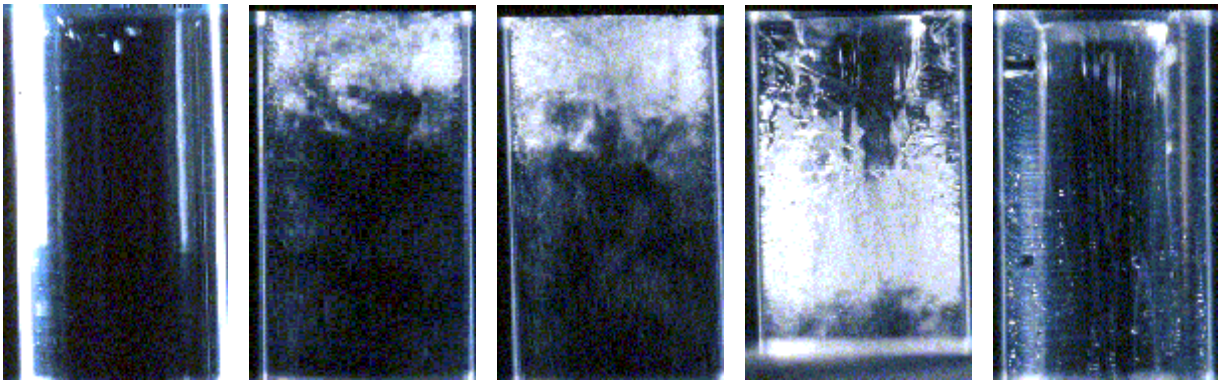

(a) (b) (c) (d) (e)

Figure 12. Cavitation structure in nozzle-D

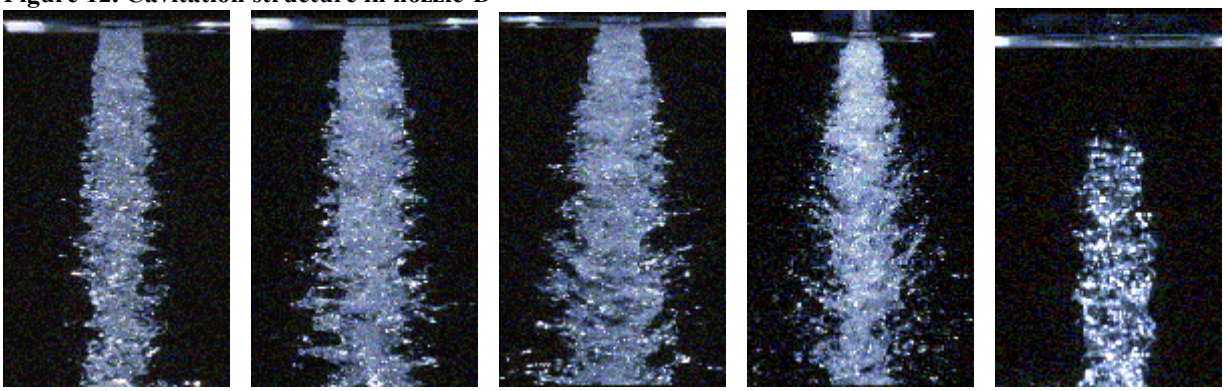

(a) (b) (c) (d) (e)

Figure 13. Spray dispersion from nozzle-D

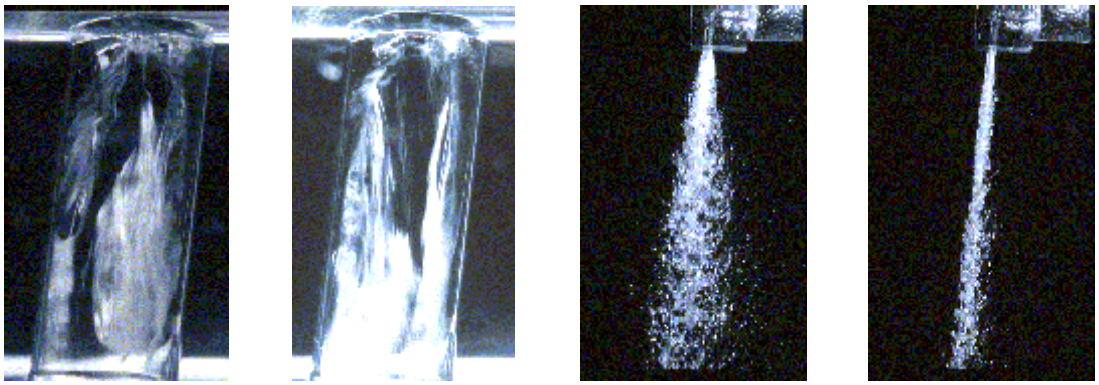

(a) (b) (c) (d)

Figure 14. Cavitation distribution and spray dispersed from nozzle-B at glassy sheet cavitation stage

As the flow was increased beyond the developed coherent structure stage, a glossy sheet structure extended almost to the hole exit, say up to 95 % of the hole length, with approximately 5 % cloud at the exit. The glossy sheet was distributed more on to the right side of the hole than on the left side of the hole for nozzle-A, which is opposite to nozzle-C. In nozzle-D it appears that only sheet prevailed inside the hole appearing to be separated from the wall as shown in Figure 12 (e).

4 Spray pattern

When the spray was viewed from the front, the spray appeared to be symmetric under all conditions thus this view is not discussed in the paper but a detailed description of the cavitation structure on the spray pattern for nozzle-A is discussed by Ganippa *et al.* (2001). The spray plumes issuing from the nozzle-A under different cavitating conditions when viewed from the side are shown in Figure 5. Under the condition (a) to (d), the spray was observed to be symmetric. In the glossy sheet cavitation stage (e) there is a clear asymmetry in the spray. In this condition of asymmetric spray, the glossy sheet was attached to the right side of the nozzle wall throughout the hole. On the other hand, a glossy sheet was also seen on the other side of the hole, but the sheet did not extend to the hole exit. In general, cavitation was distributed more to the right side of the hole compared to the left side of the nozzle-A, Figure 5 (f). This unsymmetrical cavitating flow inside the nozzle is one of the reasons for an atomizing spray on the right side and non-atomizing spray on the left side.

In nozzle-B, the cavitation was distributed more on the right compared to the left side of the hole as shown in Figure 7 (e). This unsymmetrical distribution of cavitation within the hole resulted in an asymmetrical spray of atomizing jet on the right side and non-atomizing jet on the left were the cavitation is less distributed within the hole. The geometry of nozzle-B is such that the cavitation is highly unstable; a fact resulting in a periodic atomizing and non-atomizing spray. This is illustrated in Figure 14 (c & d) showing the spray pattern corresponding to a moment at which the cavitation distribution within the hole is altered, Figure 14 (a & b). Figure 14 (a) and (c) has already been discussed in Figure 7 (e) and 8 (e) respectively.

The spray dispersion in nozzle-C is quite interesting, as we have discussed, the cavitation is distributed more on to the left side of the hole at high flow conditions this effect of uneven distribution of the cavitation cloud, causes the spray to be more dispersed on the left compared to a less dispersed one on the right as shown in Figure 11 (e).

The spray dispersion from nozzle-D is quite different in nozzle-A, B and C. It was observed that the corresponding in-hole cavitation appears as a dense cloud near the hole inlet in Figure 12 (c) and a cloud suspended at the middle of the hole by a sheet attached to the inlet in Figure 12 (d). These clouds would create an intense turbulence by imploding and causing a bushy atomizing spray, Figure 13 (c) and Figure 13 (d). As the flow is increased the suspended cloud extends to the hole exit and the sheet connecting the cloud to the hole inlet extends all the way to the exit and results in a glass like jet close to the nozzle exit which not visible in Figure 13 (e) and relatively a non-atomizing jet.

5 Discussions

The experimental results and the observations indicate that the distribution of cavitation within the hole and in some cases the cavitation structure play a vital role on the spray pattern and atomization. In the developed coherent cavitation stage, the spray appeared to be widely dispersed in nozzle-A, nozzle-B and nozzle-C. The spray issuing from the nozzle-D appeared to be more bushy when the suspended cloud moves towards the hole exit and once the cavitation cloud comes out of the hole exit there is a glass like non-atomizing jet which is also referred to as hydraulic flip. The structure of cavitation and its distribution within the hole are sensitive to the geometry of the sac and hole, which is a key fact to be considered in optimizing the spray pattern. As the hole inclination increases the cavitation shifts to the left, a tendency seen right from the incipient stage. Observations made from the present study indicate that there is a strong influence of hole inclination on the spray pattern

6 Conclusions

The cavitation phenomena and the spray structure in a transparent single nozzle having a hole inclined at 90, 85, 80 and 0 degree to the spray axis have been visualized and the following conclusions were drawn.

* In all the four nozzles the inception bubbles grew intensively in the shear layer and developed into cloud-like coherent structures.
* The instabilities of the shear layer caused the cloud cavitation structures to break off, which subsequently lead to the shedding of the cavitation cloud. The shed cavitation was similar in shape to a horseshoe vortex in nozzle-A, nozzle-B and nozzle-C. Shedding was also observed in nozzle-D.
* Under very high flow conditions the cavitation cloud can transform into a glossy sheet form.
* The non-symmetric distribution of cavitation within the hole resulted in a jet that was atomizing on one side where the cavitation was present within hole and the non-atomizing on the other side of the hole where the cavitation was less. This resulted in an asymmetric spray structure.

Acknowledgements

The authors wish to thank the Chalmers Combustion Engine Research Centre (CERC) for the financial support. The help rendered by Jan-Olof Yxell and the technical staff at the Department of Thermo and Fluid Dynamics is appreciated

References

Arcoumanis, C., Flora, H., Gavaises, M., Kampanis, N. & Horrocks, R. (1999). *SAE Paper* 1999-01-0524.

Arcoumanis, C., Badami, M., Flora, H. & Gavaises, M. (2000). *SAE Paper* 2000-01-1249.

Badock, C., Wirth, R., Fath, A. & Leipertz, A. (1998). *ICLASS-98, Manchester.*

Bergwerk, W. (1959). *Proceedings of the Institution of Mechanical Engineers,* **173(**25), 655-660.

Chaves, H., Knapp, M. & Kubitzek, A. (1996). *SAE Paper* 962004.

Ganippa, L.C., Bark, G., Andersson, S. & Chomiak, J. (2001). *SAE Paper* 2001-01-2008.

Heimgärtner, C., & Leipertz, A. (2000). *SAE Paper* 2000-01-1799.

Hiroyasu, H., Arai, M. & Shimizu, M. (1991). *ICLASS-91, Gaithersburg*, 275-282.

Kato, M., Kano, H., Date, K., Oya, T. & Niizuma, K. (1997). *SAE Paper* 970052.

Kim, J-H., Nishida, K., Yoshizaki, T. & Hiroyasu, H. (1997). *SAE Paper* 972942.

O'Hern, T.J. (1991). *Journal of Fluid Mechanics,* **215**, 365 – 391.

Reitz, R.D. & Bracco, F.V. (1982). *Phys. Fluid*, **25**(10), 1730-1742.

Soteriou, C., Andrews, R., & Smith, M. (1999). *SAE Paper* 1999-01-1486.

Taneda, S. (2000). *Journal of Fluid Dynamics Research* **27**, 335-351.

Walther, J., Schaller, J, K., Wirth, R. & Tropea, C. (2000). *ILASS-Europe, Darmstadt.*